Revista Brasileira de Ciências Ambientais
Brazilian Journal of Environmental Sciences

Chemical characteristics of size-segregated particles from a brazilian coastal megacity

Características químicas de partículas segregadas por tamanho de uma megacidade costeira brasileira

Maria Fernanda Caceres[1], *Eduarda Santa-Helena*[1], *Anna De Falco*[1], *Gabriel Gonçalves*[1], *Marcos Felipe de Souza Pedreira*[1], *Sergio Machado Corrêa*[2], *Adriana Gioda*[1]

ABSTRACT

Particulate matter (PM) size distribution samples were collected using a Micro-Orifice Uniform Deposit Impactor (MOUDI) in Rio de Janeiro between July and September 2016 during the Olympic and Paralympic periods, when there was an increase in tourist flow, changes in the local economy, modifications in traffic and pollution emission patterns. The samples were analyzed for elemental composition using inductively coupled plasma mass spectrometry (ICP-MS), for organic and inorganic ions using ion chromatography, and for polycyclic aromatic hydrocarbons (PAHs) using gas chromatography-mass spectrometry (GC/MS). The data were processed, interpreted, and discussed through statistical analyses performed in R Language, including boxplots and Pearson correlation methodology. Results were categorized according to particle size: coarse, fine, ultrafine, and nano. Chloride dominated the coarse particulate matter (PMC; 18–3.2 µm), NO_2^- the fine fraction (PMF; 1.8–0.56 µm), and $HCOO^-$ the ultrafine fraction (PMN; 320–56 nm). Ni, Pb, Sb, and V were enriched in PMN. Four- and five-ring PAHs were predominant across all particle size groups. The species present in the coarse fraction come from natural sources, while those in the fine fraction are of anthropogenic origin, mainly from the combustion of diesel and gasoline by vehicle engines.

Keywords: IC; ICP-MS; metals; MOUDI; PAHs; water-soluble ions.

RESUMO

Amostras de distribuição de tamanho de material particulado (MP) foram coletadas usando um Impactor de Depósito Uniforme de Micro-Orifício (MOUDI) no Rio de Janeiro, entre julho e setembro de 2016, durante os períodos olímpico e paralímpico, quando houve aumento no fluxo turístico, mudanças na economia local, modificações no tráfego e nos padrões de emissão de poluição. As amostras foram analisadas quanto à composição elementar usando espectrometria de massas com plasma indutivamente acoplado (ICP-MS), para íons orgânicos e inorgânicos usando cromatografia iônica e para hidrocarbonetos aromáticos policíclicos (HPA) usando cromatografia gasosa acoplada à espectrometria de massas (GC/MS). Os dados foram processados, interpretados e discutidos por meio de análises estatísticas realizadas em linguagem R, incluindo *boxplots* e metodologia de correlação de Pearson. Os resultados foram categorizados de acordo com o tamanho de partícula: grosso, fino, ultrafino e nano. O cloreto dominou o material particulado grosso (PMC; 18–3,2 µm), o NO_2^- a fração fina (PMF; 1,8–0,56 µm) e o $HCOO^-$ a fração ultrafina (PMN; 320–56 nm). Ni, Pb, Sb e V foram enriquecidos no PMN. HPA de quatro e cinco anéis foram predominantes em todos os grupos de tamanho de partícula. As espécies presentes na fração grossa são provenientes de fontes naturais, enquanto as da fração fina são de origem antropogênica, principalmente da combustão de *diesel* e gasolina por motores de veículos.

Palavras-chave: CI; ICP-MS; metais; MOUDI; HAP; íons solúveis em água.

[1]Pontifícia Universidade Católica do Rio de Janeiro (PUC-Rio) — Rio de Janeiro (RJ), Brazil.

[2]Universidade Estadual do Rio de Janeiro (UERJ) — Rio de Janeiro, RJ, Brazil.

Corresponding author: Adriana Gioda — Pontifical Catholic University of Rio de Janeiro (PUC-Rio), Department of Chemistry — Rua Marques de São Vicente 225 — Gávea — CEP: 22451-900 — Rio de Janeiro (RJ), Brazil. E-mail: agioda@puc-rio.br

Conflicts of interest: the authors declare no conflicts of interest.

Funding: this work was supported by the Coordenação de Aperfeiçoamento de Pessoal de Nível Superior – Brasil (CAPES) [Finance Code 001], FAPERJ for the Post-Doc fellowship (E-26/202.314/2019 and E-26/202.020/2020, respectively). FAPERJ (Auxílio Cientista do Nosso Estado) and CNPq (Bolsa de Produtividade).

Received on: 04/05/2025. Accepted on: 10/30/2025.

https://doi.org/10.5327/Z2176-94782543

Introduction

Atmospheric pollution refers to the qualitative and quantitative presence of various compounds in the air that differ from established local or international standards and legislation, and that exhibit varying levels of toxicity (Konieczka et al., 2022). Technological advancement and the exploitation of natural resources have significantly contributed to atmospheric pollution, exacerbating phenomena such as the greenhouse effect and acid rain deposition (Zhang et al., 2004; Patel and Jiang, 2021), as well as increasing the incidence of diseases, especially those affecting the cardiorespiratory system (Cortés et al., 2022; Casela et al., 2023; Requia et al., 2023; Buya et al., 2024; Zhang et al., 2024) and the immune system (Rodríguez-Cotto et al., 2014).

One approach to assessing pollution levels is through the sampling and analysis of atmospheric air, particularly focusing on particulate matter (PM), which is one of the primary pollutants resulting from combustion processes (Wang et al., 2022). PM generated has raised global concern due to its adverse health effects, including damage to the upper respiratory tract (Ottaviano et al., 2022), vascular issues (Hantrakool et al., 2022), general toxicity (Jairi et al., 2025), and inflammatory responses (Koo et al., 2024). Vehicular emissions are the major contributor of PM in urban areas, besides hundreds of volatile organic compounds (VOCs), including oxygenated and sulfur-containing species (Hopke and Hidy, 2022; Fu et al., 2023). The physical and chemical characteristics of PM depend on multiple factors, such as fuel type, engine configuration, operating conditions, vehicle maintenance, age, and post-combustion technologies (Verma et al., 2014, 2019; Corrêa et al., 2021). In Brazil, fuel and vehicle technologies have evolved over the years as part of legislation and emission control measures, thereby influencing air quality in urban centers.

PM can be found in either solid or liquid form, suspended in the atmosphere, and varies in chemical composition and size, ranging from a few nanometers to several micrometers (Lee et al., 2019; Bellouin, 2026). In terms of air quality assessment, PM is typically categorized as PM_{10} (with diameters of 10 µm or less) and $PM_{2.5}$ (with diameters of 2.5 µm or smaller), which are monitored by high-volume (Hi-Vol) samplers or in automated monitoring stations (Orellano et al., 2020). However, particles in other size ranges, particularly in the nanometric scale, are not routinely monitored by environmental agencies. Instead, their characterization is carried out by research institutions and specialized laboratories. Instruments such as the Micro-Orifice Uniform Deposit Impactor (MOUDI) and the Dekati® Low Pressure Impactor (DLPI+) are commonly used to separate and analyze airborne particles by size. The MOUDI operates with eight or ten stages and collects particles in the size range of 0.056 to 18 µm. The DLPI+, on the other hand, is a 14-stage cascade impactor that classifies and collects particles into 14 size fractions ranging from 16 to 10 µm, enabling detailed analysis of particle mass size distribution in the atmosphere. Currently, these equipments are available in other versions with different configurations.

In Brazil, studies on air quality concerning ultrafine particles are still limited. Silveira et al. (2022) analyzed metal and polycyclic aromatic hydrocarbon (PAHs) concentrations present in PM down to the nanometer scale sampled in the central region of Rio de Janeiro. Similarly, Souza et al. (2021) investigated the presence of metals associated with size-fractionated PM in the northern zone of Rio de Janeiro. Both studies confirmed the presence of these pollutants across all particle size ranges. Additionally, Rocha and Corrêa (2018) evaluated metal emissions from diesel engines operating with varying biodiesel concentrations. Studies were also carried out in São Paulo with MOUDI to monitor metals and black carbon (Sánchez-Ccoyllo et al., 2009; Albuquerque et al., 2012).

The present study aimed to quantify selected organic and inorganic species in size-segregated particles collected in the southern region of Rio de Janeiro city using a MOUDI sampler, to evaluate the impact of the Olympic Games on local air quality. Atypical events like these significantly alter the concentrations of primary pollutants. The chemical analyses were performed using chromatographic and spectrometric techniques. To the best of our knowledge, this is the first study in Rio de Janeiro to employ such a combination of methodologies to characterize atmospheric PM at this level of detail.

Methodology

Sampling

To collect size-segregated PM, a MOUDI, model 120R (MSP Corporation, USA) was employed, featuring ten nominal aerodynamic cut-off diameters: 0.056, 0.100, 0.180, 0.320, 0.560, 1.000, 1.800, 3.200, 5.600, 10.000, and 18.000 µm. The MOUDI sampler was installed on the rooftop of a 7-story building at the Pontifical Catholic University of Rio de Janeiro (PUC-Rio) (22°58'43.8"S, 43°13'59.7"W). The sampling site was strategically located near tunnels and high-traffic roadways, close to water bodies such as Rodrigo de Freitas Lagoon and the Atlantic Ocean, and adjacent to the Tijuca Forest, the largest urban rainforest in the world. It is important to note that this tunnel connects the South Zone to the West Zone, linking both areas where the Olympic arenas were located. For sample collection, 47 mm polytetrafluoroethylene (PTFE) membrane filters (Fluopore™), for ions and elements, and aluminum substrates, for PAHs, were used, at a constant flow rate of 30 L min^{-1}. Sampling was carried out over six weeks, from July to September 2016, during the Olympic and Paralympic Games. Each sampling period lasted between 48 and 96 hours. This extended sampling period, compared to the standard 24-hour reference, was necessary because the flow is lower and particles are size-fractionated, leading to lower concentrations and potentially hindering the detection of chemical components.

Chemical analyses

Fifty-five filters, corresponding to five sampling periods (n=5), were analyzed to determine ions and metals, as planned in the experimental design. However, during the sampling campaign, the opportunity arose to analyze PAHs, and therefore, we kept only one sample (11 filters, n=1) as a test. Whole filters were extracted with 10 mL of ultrapure water (GenPure, Thermo ScientificTM) and shaken by in vortex (Biomixer, Brazil) for 5 minutes. Subsequently, the tubes were placed in an ultrasound bath for 45 minutes and left in a stirring tray for 1 hour. The resulting solution was centrifuged, and the supernatant was analyzed on an ICS 5000 dual ion chromatography system (Thermo Scientific Dionex, USA) for the determination of anions (Fl^-, Cl^-, NO_2^-, Br^-, NO_3^-, SO_4^{2-}, PO_4^{3}, CH_3COO^-, $HCOO^-$, $CH_2(COO)_2^{2-}$, and $C_2O_4^{2-}$) and cations (Li^+, Na^+, K^+, NH_4^+, Mg^{2+}, and Ca^{2+}) (Justo et al., 2019). Anions were analyzed on a Dionex IonPac AS19 column (Thermo Scientific Dionex, Massachusetts, USA) eluted with KOH, while cations were analyzed on a Dionex IonPac CS 12A column (Thermo Scientific Dionex, Massachusetts, USA) and a micromembrane suppressor eluted with CH_3SO_2OH (18.0 mmol L^{-1}). The AS-AP temperature was set to 10°C to minimize the loss of volatile compounds. For the quantification, analytical curves were prepared by the external calibration method from individual standards of 1000 mg L^{-1} (Sigma-Aldrich, USA). Standard solutions with a concentration of 150 µg L^{-1} of the ion mixture were analyzed for every ten samples to corroborate the analytical curve during the analyses. Limits of detection (LOD) and quantification (LOQ) were calculated from the results of three blank filters analyzed in triplicate. The instrumental detection and quantification limits were considered for the ions not detected in the blanks, calculated from the lowest concentration level in the analytical curve.

After the aqueous extraction, the same filter was transferred to a new 50 mL polyethylene tube, and 3 mL of bidistilled HNO_3 was added and heated at 100°C for 2 hours. The extracts were diluted in water and analyzed in a NexIon 300X Inductively Coupled Plasma Mass Spectrometer (PerkinElmer-Sciex, USA). The supernatants obtained from the aqueous extraction were also analyzed to determine 60 elements. Analytical curves of the elements of interest were prepared in a 5% v/v HNO_3 solution in the concentration range from 0.001 to 80.000 µg L^{-1} to quantify elements. Standard multi-element stock solutions PE5, PE29 and PE12 (Perkin Elmer, USA) were used to prepare the solutions. A Rh solution (40 µg L^{-1}) was used as the internal standard, injected in line with all solutions (Justo et al., 2019). The operating conditions of the equipment were verified through monitoring parameters such as the signal intensities of In, Mg and Y elements, the formation of oxides through the CeO^+/Ce^+ ratio, and the formation of bivalent species through the Ba^{2+}/Ba ratio. The limits of detection and quantification were calculated from the results obtained from the analysis of ten blank solutions with 10% HNO_3.

PAHs were determined in the samples collected in the aluminum substrates (n=1). The filters were immersed in 5 mL of a 1:1 mixture of acetonitrile and dichloromethane and subjected to an ultrasound bath for 30 min, a procedure repeated twice. Filter extracts were grouped according to their size into three groups as follows: 18–3.20 µm (Coarse — PMC), 1.80–0.56 µm (Fine — PMF) and 0.32–0.56 µm (Nano — PMN). The selected size ranges are directly related to the MOUDI cutoff points. Each group's solutions were transferred to a volumetric flask, and the filters were washed with a mixture of solvents. The resulting solution was rotovaporated at a temperature of 40°C until reaching a final volume of 2 mL, using nitrogen flow. Subsequently, the supernatant was taken, transferred to a vial, and analyzed in a gas chromatograph coupled with a mass spectrometer (Varian 450GC MS220 PTV 1079). For the analysis, 2.0 µL were injected at 320°C in splitless mode. The oven temperature began at 70°C, maintained for 2 minutes, followed by a heating rate of 12°C min^{-1} up to 320°C, which was maintained for 8 minutes (Casal et al., 2014; Souza and Corrêa, 2015, 2016). The mobile phase was Helium 5.0 at a constant flow of 1.2 mL min^{-1}. The chromatograph column was Supelco SLB 5MS (30 m, 0.25 mm, 0.25 µm). The temperatures of the MS were 250, 40, and 280°C for the transfer line, manifold, and ion trap, respectively.

Nine PAHs were determined in the PM phase, including anthracene (ANT), phenanthrene (PHE), fluoranthene (FLT), pyrene (PYR), benzo[a]anthracene (BaA), chrysene (CRY), benzo[b]fluoranthene (BbF), benzo[k]fluoranthene (BkF), and benzo[a]pyrene (BaP). The monitored ions (m/z) were 177–178 for PHE and ANT, 202-203 for FLT and PYR, 225-230 for BaA, 250-260 for BbF, BkF and BaP. For all ions the filament current was 40 µA. For the quantification of the analytes, analytical calibration curves were prepared using standard solutions of the PAHs (Supelco EPA 610-N PAH kit 47351) at five different concentration levels from 10 to 200 µg L^{-1}, using the external standard technique in duplicate injections. The LOD was calculated by multiplying the linear coefficient's standard deviation by 3.3 and dividing by the angular coefficient. The LOQ was calculated by multiplying the LOQ by 10.

Statistical data treatment

Data were treated using the R Language (R Core Team, 2020) for descriptive and multivariate analyses. For descriptive analyses, boxplots were used to validate data, but the measured values were presented in the form of a barplot with the standard deviation. Data were grouped and analyzed by correlation matrices using Pearson methodology (Härdle and Simar, 2015).

Results and Discussion

Since many chemical species were not detected across all particle size fractions, the fractions were combined to allow a more robust interpretation of the results. To characterize the collected samples, PM was cate-

gorized into three size fractions: Coarse (PMC — 18.0, 10.0, 5.6, and 3.2 µm), Fine (PMF — 1.80, 1.00, and 0.56 µm), and Nanoparticles (PMN — 320, 180, 100, and 56 nm). Figure 1 presents the identified ions in each PM fraction, with their distribution according to particle size. Detailed quantitative results are provided in Table SM1 (Supplementary Material).

Chloride was the predominant ion in the PMC, NO_2^- in the PMF, and $HCOO^-$ in the PMN. Other ions also contributed substantially, such as Mg^{2+} and Na^+ in PMC; Ca^{2+} and $C_3H_2O_4^{2-}$ in PMF; and NH_4, $(C_2O_4)^2$, and SO_4^{2-} in PMN. Considering ions with mean concentrations above 100 ng m^3, seven were identified in PMC, five in PMF, and four in PMN. Ammonium in PMC and F^- in PMN were below the LOD, and fourteen ions presented mean concentrations below 10 ng m^{-3}. On average, ions associated with the PMC accounted for 57.2% of the total, while those in the PMF and PMN represented 23.8 and 19.0%, respectively.

Nitrate was only detected in particles within two size ranges: 0.18 µm and between 1.0 and 1.8 µm, with concentrations ranging from 58 to 73 ng m^{-3}. Nitrate emissions are a combination of sources, from the natural nitrogen cycle to burning processes. Sodium showed its highest concentrations in particles ranging from 0.56 to 3.2 µm, while SO_4^{2-} was most abundant in the ultrafine range, particularly between 0.056 and 0.1 µm. Magnesium exhibited its highest concentrations in particles ranging from 1.0 to 3.2 µm. Oxalate was the water-soluble organic anion with the highest concentration detected across the different particle size fractions. Its highest concentrations were found in the smallest particles (0.056–0.18 µm), with presence also observed in the 18 µm fraction. Oxalate is released in greater quantities into the atmosphere through the dispersion of dust particles and in smaller quantities through biological processes.

Among the cations analyzed, NH_4^+ and K^+ had concentrations above the LOD in the 0.056–0.1 µm size range, which was also where their concentrations peaked. Waste incineration, the natural nitrogen cycle as part of the organic decomposition process and combustion by combustion engines emit ammonia, converted to ammonium. Potassium was additionally detected in the 0.56 µm and 10 µm fractions, typically of natural origin. The highest concentration of Ca^{2+} was determined in the fine fraction, demonstrating the contribution of the numerous civil construction activities in the region.

Ions derived from natural processes, such as those from the sea (Na^+, Cl^-, Mg^{2+}, K^+) and soil (Ca^{2+}, Mg^{2+}, K^+, carbonates, silicates, mineral dust), are usually found in the coarse mode of aerosols. This occurs because they enter the atmosphere already as relatively large fragments, such as sea spray droplets or solid particles resuspended from the soil and therefore do not undergo the nucleation-condensation process that generates ultrafine and fine particles. In contrast, ions derived from combustion processes or secondary chemical reactions (*e.g.*, SO_4^{2-}, NO_3^-, NH_4^+) are predominantly present in the fine mode. These species are formed from gaseous precursors (SO_2, NO_x, NH_3, volatile organic compounds) that undergo oxidation in the gas phase and subsequently condense or nucleate to form small particles.

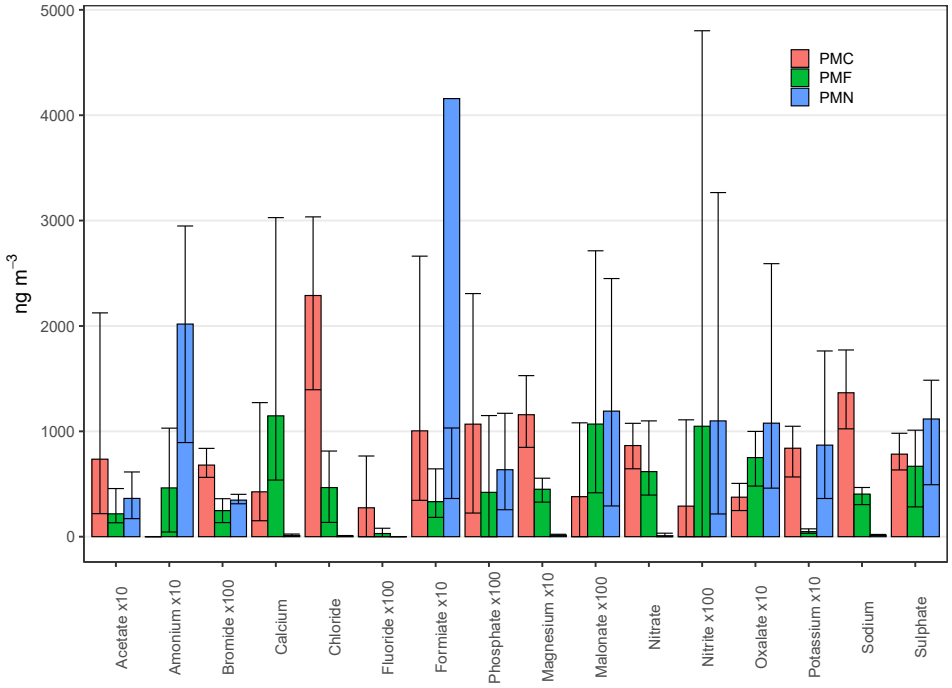

Figure 1 – Concentrations of soluble ions grouped by particle size ranges: Coarse — PMC (18, 10, 5.6, and 3.2 µm), Fine — PMF (1.8, 1.0, and 0.56 µm), and Nano — PMN (320, 180, 100, and 56 nm) (n=5).
PMC: Coarse Particulate Matter; PMF: Fine Particulate Matter; PMN: Nano Particulate Matter.

Figure 2 presents the elemental composition results for the sum of aqueous and acid extracts. Of the 60 elements analyzed, only 17 showed concentrations above the LOD, with 13 of them predominantly found in the PMC. Elements such as Ni, Pb, Sb, and V were more concentrated in PMN, representing a higher potential health risk due to their ability to penetrate deeper into the respiratory system. Elements such as Fe, Si, Al, Ti, Ca, Ba, and Zn are predominantly found in the coarse particle fraction because they are mainly associated with crustal and mechanical sources that generate larger particles through physical processes rather than by secondary atmospheric formation. Crustal elements like Fe, Si, Al, and Ti originate from soil dust, mineral particles, and road dust resuspension, which typically occur in the micrometer size range. Similarly, Zn, as well as Fe, is strongly linked to traffic-related mechanical abrasion processes, such as tire and brake wear, which release particles mostly in the coarse mode. In contrast, elements derived from combustion and secondary processes (*e.g.*, Pb, Ni, V) are more often associated with the fine fraction, as they originate from vapor-phase emissions that condense or nucleate into smaller particles. Detailed results are provided in Table SM2.

Analysis of the elemental composition of PM by particle size (Figure 2) revealed that the 0.32 µm fraction contained the largest number of detected metals. Among them, Ca showed the highest concentrations (PMC), reaching 71 ng m^{-3}, followed by Fe (PMC). Calcium showed contrasting distributions depending on the extraction method. In the water-soluble fraction, it was mainly present in fine particles, likely as secondary salts such as $Ca(NO_3)_2$, $CaCl_2$, or partially soluble $CaSO_4$. Under acid extraction, however, Ca was predominantly found in the coarse fraction, reflecting its occurrence in insoluble minerals like $CaCO_3$ and silicates from crustal or resuspended dust. This behavior indicates the coexistence of secondary soluble species in the fine mode and primary mineral phases in the coarse mode. Si was also found in most of the particle size fractions, except in those of 0.056, 0.56, 1.0, and 10 µm. Its highest concentration (118 ng m^{-3}) was observed in the 0.1 µm fraction. Potassium and Zn were only detected above the LOD in the 0.18 and 0.32 µm fractions, with concentrations of 8.7 and 7.5 ng m^{-3} for K, and 3.2 and 2.6 ng m^{-3} for Zn, respectively. Mn and Pb were found in only a few samples, where Mn was detected above the LOD in particles with aerodynamic diameters of 1.8 and 5.6 µm, while Pb was only present in the 0.056 and 0.1 µm fractions. Nickel was the only trace element in this group consistently found across all particle sizes. Its highest concentrations were recorded in the 0.1, 1.8, and 3.2 µm fractions, with values of 0.23, 0.52, and 0.23 ng m^{-3}, respectively; the remaining fractions showed concentrations ranging from 0.05 to 0.12 ng m^{-3}. The 0.056 µm fraction exhibited the highest diversity of trace metals among Ni, Ba, and Pb, with Ba presenting the highest concentration (0.64 ng m^{-3}). In contrast, only Ni was detected in the 0.56 and 10 µm samples, both with concentrations of 0.06 ng m^{-3}. The main fuels in Brazil are gasoline (73% gasoline and 27% anhydrous ethanol), ethanol, and diesel (a blend of petroleum diesel with 9% biodiesel). Trace metals can be presented at vehicle fuels like gasoline, ethanol,

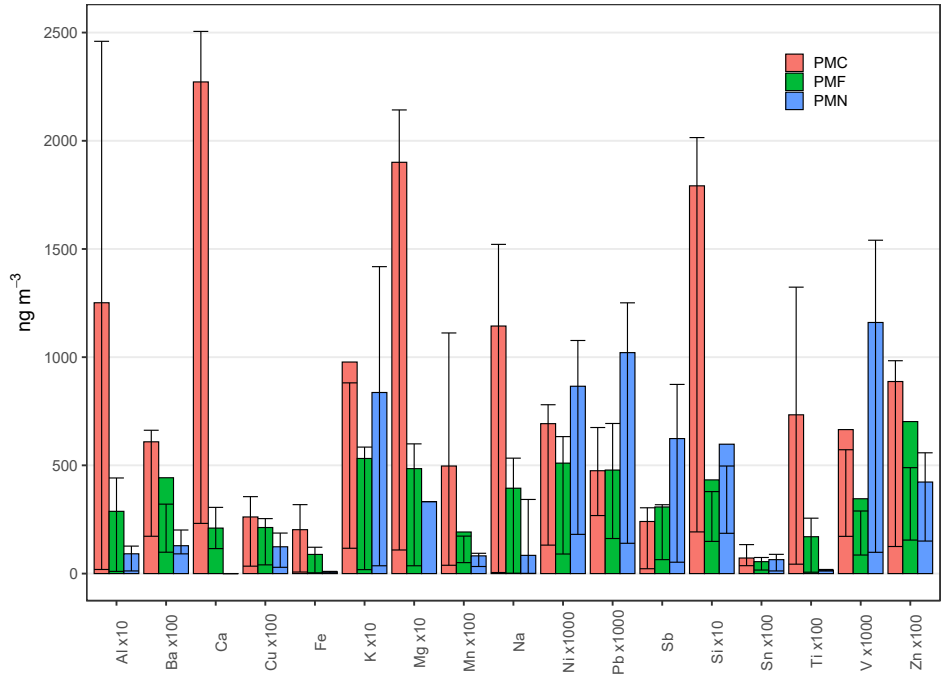

Figure 2 – Concentration of trace elements in particulate matter samples by particle size fraction, based on the sum of aqueous and acid extracts. Coarse — PMC (18, 10, 5.6, and 3.2 µm), Fine — PMF (1.8, 1.0, and 0.56 µm), and Nano — PMN (320, 180, 100, and 56 nm) (n=5).
PMC: Coarse Particulate Matter; PMF: Fine Particulate Matter; PMN: Nano Particulate Matter.

and diesel. These metals typically come from external sources rather than being part of the fuel's natural composition. In gasoline, contaminants such as Fe, Cu and Ni are often introduced when the fuel comes into contact with storage tanks and pipes. Similarly, diesel can contain V, Ni, Fe, Cu and Zn, which are either present in the crude oil or result from engine wear, and lubricating oil. Ethanol and biodiesel, on the other hand, can have trace metals from their production processes. Ethanol may contain residual K, Ca, Mg, and Na from agricultural inputs and Cu from its production. In biodiesel, these same metals are often left over from the catalysts used during the transesterification process.

The results obtained are comparable, in terms of the predominance of chemical species, to those reported in a study conducted in Gávea between July and September 2016 (Justo et al., 2019). The major ions identified in PM_{10} were Na^+ (2.74±0.98 μg m^{-3}), Cl^- (3.86±3.18 μg m^{-3}), and SO_4^{2-} (2.61±1.22 μg m^{-3}). The main trace elements detected included Fe (124 ± 62 ng m^{-3}), Cu (15.6±9.2 ng m^{-3}), Ti (3.09±2.34 ng m^{-3}), and Mn (2.21±1.18 ng m^{-3}). These findings are also consistent with those of another study carried out in Rio de Janeiro with a similar scope (Beringui et al., 2021). The chemical composition of the different PM fractions was similar to that reported in a study conducted in São Paulo (Albuquerque et al., 2012), particularly with respect to trace elements. Comparable results were also observed in studies on vehicular PM emissions from highway tunnels in São Paulo (Sánchez-Ccoyllo et al., 2009). However, few studies have investigated elemental composition by stratified particle size in Rio de Janeiro. Silveira et al. (2022) analyzed 13 elements in downtown during 2019–2020 using the same sampling methodology. They grouped the ten MOUDI stages into four size categories: coarse (PMC), fine (PMF), ultrafine (PMUF), and nano (PMN). In the PMC fraction, Fe and Ca were the predominant elements, consistent with our findings. For PMF and PMUF, Fe, Ca, Cu, Mn, and Zn were dominant, while Mn was the main element identified in the PMF fraction. Souza et al. (2021) also conducted a study in the northern zone using the same sampling approach. The average mass concentrations for PMN, PMUF, PMF, and PMC were 11.8, 8.2, 7.7, and 7.1 μg m^{-3}, respectively. Furthermore, the mean concentrations of Cd, Ni, Pb, Cr, and Fe were in compliance with the U.S. EPA air quality standards for $PM_{2.5}$ (0.0002, 0.00024, 0.5, 0.012, and 10 μg m^{-3}, respectively).

In addition to metals and inorganic ions, PAHs were also quantified across the three particle size modes (Figure 3). The results indicated that PAHs containing four and five aromatic rings exhibited the highest concentrations in all particle size fractions. In contrast, PAHs composed of three and four rings accounted for less than 10% of the total PAH concentrations detected.

The concentrations of the heaviest PAHs, as well as BaA, were slightly higher in the PMF and PMN fractions compared to PMC. The predominant PAH compounds identified were the isomers BbF, BkF, and BaP, although PMN exhibited the lowest relative contribution among the three size fractions. Diagnostic ratios were applied to assess the potential sources of PAHs (Wang et al., 2016c), distinguishing between petrogenic and pyrogenic origins, following methodologies proposed by Lin et al. (2021) and Lohmann et al. (2024), as summarized in Table 1. The ratios were obtained based on Guanabara Bay, one of the main oceanic bays located in the state of Rio de Janeiro.

The BaA/(BaA+CRY) ratio found in this study, close to 0.50 across all PM size fractions, suggests a mixed contribution from both diesel and gasoline emissions. According to Ravindra et al. (2008), values below 0.50 indicate a predominance of diesel emissions, whereas values above 0.50 point to gasoline sources. This ratio also confirms a contribution from both lighter and heavier vehicles, given the nearly balanced proportion of benzo anthracene and chrysene. A similar interpretation applies to the FLT/(FLT+PYR) ratio where values below 0.50 are typically as-

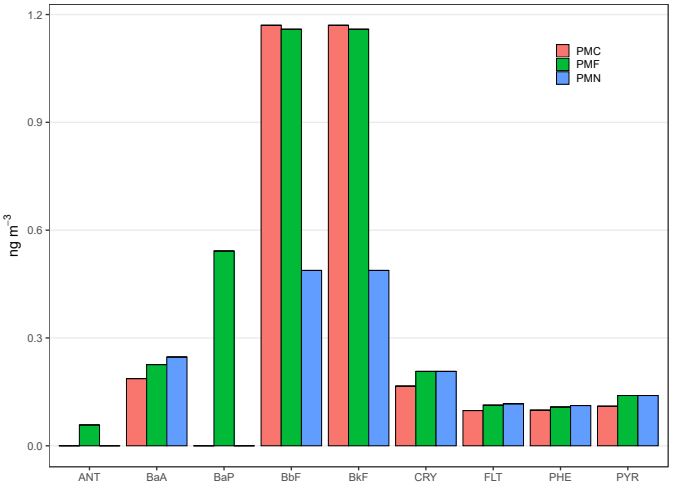

Figure 3 – Concentrations of polycyclic aromatic hydrocarbons grouped by particle size ranges: Coarse — PMC (18.0, 10.0, 5.6, and 3.2 μm), Fine — PMF (1.80, 1.00, and 0.56 μm), and Nano — PMN (320, 180, 100, and 56 nm) (n=1).

PMC: Coarse Particulate Matter; PMF: Fine Particulate Matter; PMN: Nano Particulate Matter.

Table 1 – Values of diagnostic ratios for polycyclic aromatic hydrocarbon concentrations.

Diagnostic Ratio	PMC	PMF	PMN
BaA/(BaA+CRY)	0.53	0.52	0.54
FLT/(FLT+PYR)	0.47	0.45	0.46
ANT/(ANT+PHE)	-	0.35	-

PMC: Coarse Particulate Matter; PMF: Fine Particulate Matter; PMN: Nano Particulate Matter.

sociated with diesel emissions, while higher values are linked to gasoline combustion. Once again, the results suggest that local emissions originate from a combination of fuel sources (Rogula-Kozłowska et al., 2013). The similar ratio for the three sample sizes shows a lower proportion of fluoranthene in relation to pyrene, thus highlighting the burning of fuels of petroleum origin. Furthermore, as reported by Pies et al. (2008), the ANT/(ANT+PHE) ratio can be used to differentiate between petrogenic and pyrogenic sources. Values below 0.10 indicate petrogenic origins, whereas values above this threshold suggest pyrogenic sources. The result confirms that the fine fraction has a higher amount of anthracene compared to phenanthrene. These compounds are characteristic markers of urban centers, which have significant emissions from fossil fuels.

Among the PAHs detected in the samples, those composed of four and five aromatic rings, such as BaA, BaP, CRY, BbF, and BkF, are particularly concerning due to their carcinogenic and teratogenic properties, which may lead to genetic abnormalities (Jakovljevic et al., 2025). These compounds are predominantly associated with fine particles, especially those smaller than 2 µm in aerodynamic diameter (Wang et al., 2016a, 2016b). Considering the characteristics of the sampling site in Gávea, the anthropogenic contributions are most significant, particularly from vehicular traffic and the combustion of fossil fuels, such as gasoline and diesel. The presence of PAHs associated with diesel vehicle exhaust, as well as in diesel fuel and engine lubricating oil, has been confirmed in similar studies reported in the literature (Souza and Corrêa, 2016).

Our study was conducted during the Olympic period, a time characterized by unique emission patterns and specific atmospheric conditions in Rio de Janeiro. When compared with the other studies, some differences in concentration levels become evident (Table SM3, Supplementary Material). Our results showed higher concentrations of Fe and Mn in the PMC and PMF fractions, as well as elevated Cu in both PMF and PMN fractions. In contrast, Silveira et al. (2022) reported substantially higher levels of V across all size fractions, reflecting a stronger influence of fossil fuel combustion. Meanwhile, Souza et al. (2021) presented the highest concentrations of Pb and Ni, suggesting a different emission profile, possibly associated with local industrial or vehicular sources. These variations indicate that the Olympic period exhibited a distinct chemical composition of PM, influenced not only by changes in urban dynamics and traffic restrictions but also by differences in source contributions when compared to non-Olympic scenarios. Our study shows BaA/(BaA+CRY) similar in all fractions (0.53; 0.52; 0.54), indicating a mixed contribution from both diesel and gasoline, without a strong size-dependent shift, i.e., the source mix appears relatively consistent from coarse to ultrafine particles. In parallel, FLT/(FLT+PYR) values remain <0.50 (0.47; 0.45; 0.46), which lead toward a diesel-dominated signature; taken together with the ~0.5 BaA ratio, this points to a primarily diesel influence tempered by non-negligible gasoline inputs. For comparison, Silveira et al. (2022) reported BaA/(BaA+CRY) that tilts gasoline-like in PMC (0.58) but diesel-like in PMF and PMN (0.43; 0.37), while their FLT/(FLT+PYR) is also <0.50 (0.45; 0.44; PMN<LOQ), reinforcing a diesel-skewed profile overall with a coarse-fraction nuance toward gasoline. The ANT/(ANT+PHE) ratio further supports pyrogenic (combustion) sources in both datasets (our PMF=0.35; Silveira et al. [2022] PMF=0.23), consistent with traffic-derived emissions. As always, these ratios can be modulated by atmospheric aging (*e.g.*, photodegradation, phase partitioning), but the convergent evidence here, near-0.5 BaA/(BaA+CRY) plus sub-0.5 FLT/(FLT+PYR), indicates a diesel-leaning, mixed-traffic source profile for our study period across all particle sizes.

Conclusion

This study provided a comprehensive characterization of the size-resolved chemical composition of PM collected in Gávea, Rio de Janeiro, during the 2016 Olympic and Paralympic Games (July–September). The results revealed a clear dominance of sea salt components (Cl^- and Na^+) in PMC, secondary inorganic aerosols (SO_4^{2-} and NO_3^-) in PMF and PMN, and trace elements such as Ni, Pb, Sb, and V primarily in PMN, indicating potential anthropogenic sources. The results are consistent with other studies in the literature in regions with similar characteristics, including Gávea itself. Diagnostic ratio analyses further suggested a mixed origin of PAHs from both diesel and gasoline combustion, consistent with the site's proximity to high-traffic roadways. The statistical interpretation of the results for ions, metals and PAHs, together with these tools, made it possible to highlight the increase in air pollution during the atypical event in the city, as well as to present the potential local emission sources and external contributions.

Authors' contributions

Caceres, M.F: conceptualization, data curation, formal analysis, acquisition, investigation, methodology, writing – original draft. **Helena**, E.S.: conceptualization, data curation, formal analysis, visualization, writing – original draft, writing – review & editing. **Falco**, A.: conceptualization, data curation, formal analysis, visualization, writing – original draft, writing – review & editing. **Gonçalves**, G.: writing – review & editing. **Pedreira**, M.F.S.: conceptualization and writing – review & editing. **Corrêa**, S.M.: formal analysis, methodology, resources, writing – review & editing. **Gioda**, A.: conceptualization, formal analysis, project administration, supervision, writing – original draft, review & editing.

References

Albuquerque, T.T.A.; Andrade, M.F.; Ynoue, R.Y., 2012. Characterization of atmospheric aerosol in the city of São Paulo, Brazil: comparisons between polluted and unpolluted periods. Environmental Monitoring Assessment, v. 184, 969-984. https://doi.org/10.1007/s10661-011-2013-y.

Bellouin, N., 2026. Climatology of Tropospheric Aerosols, Encyclopedia of Atmospheric Sciences. 3rd edition. Academic Press, pp. 41-49. https://doi.org/10.1016/B978-0-323-96026-7.00010-2.

Beringui, K.; Quinajo, M.F.C.; Justo, E.P.S.; Ventura, L.M.B.; Gioda, A., 2021. Assessment of the concentration and inorganic composition of particulate matter collected in the state of Rio de Janeiro. Química Nova, v. 44, 6. https://doi.org/10.21577/0100-4042.20170717.

Buya, S.; Lim, A.; Saelim, R.; Musikasuwan, S.; Choosong, T.; Taneepanichskul, N., 2024. Impact of air pollution on cardiorespiratory morbidities in Southern Thailand. Clinical Epidemiology and Global Health, v. 25. https://doi.org/10.1016/j.cegh.2023.101501.

Casal, C.S.; Arbilla, G.; Correa, S.M., 2014. Alkyl polycyclic aromatic hydrocarbons emissions in diesel/biodiesel exhaust. Atmospheric Environment, v. 96, 107-116. https://doi.org/10.1016/j.atmosenv.2014.07.028.

Casela, C.; Kiles, F.; Urquhart, C.; Michaud, D.S.; Kirwa, K.; Corlin, L., 2023. Methylomic, proteomic, and metabolomic correlates of traffic-related air pollution in the context of cardiorespiratory health: a systematic review, pathway analysis, and network analysis. Toxics, v. 11, 12. https://doi.org/10.3390/toxics11121014.

Corrêa, S.M.; Arbilla, G.; Silva, C.M.; Da Martins, E.M.; Souza, S.L.Q., 2021. Determination of size-segregated polycyclic aromatic hydrocarbon and its nitro and alkyl analogs in emissions from diesel-biodiesel blends. Fuel, v. 283, 118912. https://doi.org/10.1016/j.fuel.2020.118912.

Cortés, S.; Leiva, C.; Ojeda, M.J.; Bustamante-Ara, N.; Wambaa, W.; Dominguez, A.; Salvo, C.P.; Peralta, C.R.; Arenas, B.R.; Mesa, D.V.; Ahumada-Padilla, E., 2022. Air pollution and cardiorespiratory changes in older adults living in a polluted area in central Chile, v. 16. https://doi.org/10.1177/11786302221107136.

Fu, Z.Q.; Wu, Y.M.; Zhao, S.; Bai, X.X.; Liu, S.H.; Zhao, H.Y.; Hao, Y.; Tian, H.Z., 2023. Emissions of multiple metals from vehicular brake linings wear in China, 1980-2020. Science of The Total Environment, v. 889. https://doi.org/10.1016/j.scitotenv.2023.164380.

Hantrakool, S.; Kumfu, S.; Chattipakorn, S.C.; Chattipakorn, N., 2022. Effects of particulate matter on inflammation and thrombosis: past evidence for future prevention. International Journal of Environmental Research and Public Health, v. 19, 14. https://doi.org/10.3390/ijerph19148771.

HÄRDLE, Wolfgang Karl; SIMAR, Léopold, 2015. Applied multivariate statistical analysis. 4. ed. Springer, Heidelberg.

Hopke, P.K.; Hidy, G., 2022. Changing emissions results in changed PM2.5 composition and health impacts. Atmosphere, v. 13, 2. https://doi.org/10.3390/atmos13020193.

Jairi, I.; Rekbi, A.; Bem-Othman, S.; Hammadi, S.; Canivet, L.; Zgaya-Biau, H., 2025. Enhancing particulate matter risk assessment with novel machine learning-driven toxicity threshold prediction. Engineering Applications of Artificial Intelligence, v.139. https://doi.org/10.1016/j.engappai.2024.109531.

Jakovljevic, I.; Strukil, Z.S.; Pehnec, G.; Horvat, T.; Sankovic, M.; Sumanovac, A.; Davila, S.; Racic, N.; Gajski, G., 2025. Ambient air pollution and carcinogenic activity at three different urban locations. Ecotoxicology and Environmental Safety, v. 289. https://doi.org/10.1016/j.ecoenv.2025.117704.

Justo, E.P.S.; Quijano, M.F.C.; Beringui, K.; Saint'Pierre, T.D.; Gioda, A., 2019. Assessment of Atmospheric PM10 Pollution Levels and Chemical Composition in Urban Areas near the 2016 Olympic Game Arenas. Journal of the Brazilian Chemical Society, v. 31, 5. https://doi.org/10.21577/0103-5053.20190270.

Konieczka, A.; Adamski, M.; Dabrowski, A.; Dabrowska, A.; Jankowski, T., 2022. Distributed air pollution measurement system. Przeglad Elektrotechniczny, v. 98, 127-130. https://doi.org/10.15199/48.2022.01.25.

Koo, J.; Sim, W.J.; Lim, W.; Lim, T.G., 2024. Activation of mixed lineage kinase 3 by fine particulate matter induces skin inflammation in human keratinocytes. Toxicology Letters, v. 402, 38-43. https://doi.org/10.1016/j.toxlet.2024.11.002.

Lee, S.-H.; Gordon, H.; Yu, H.; Lehtipalo, K.; Haley, R.; Li, Y.; Zhang, R., 2019. New particle formation in the atmosphere: From molecular clusters to global climate. Journal of Geophysical Research: Atmospheres, v. 124 (13), 7098-7146. https://doi.org/10.1029/2018JD029356.

Lin, Y.; Gao, X.Y.; Qiu, X.H.; Liu, J.M.; Tseng, C.H.; Zhang, J.J.; Araujo, J.A.; Zhu, Y.F., 2021. Urinary carboxylic acid metabolites as possible novel biomarkers of exposures to alkylated polycyclic aromatic hydrocarbons. Environmental International, v. 147. https://doi.org/10.1016/j.envint.2020.106325.

Lohmann, R.; Vrana, B.; Muir, D.; Smedes, F.; Sobotka, J.; Zeng, E.Y.; Bao, L.J.; Allan, I.J.; Astrahan, P.; Bidleman, T.; Crowley, D.; Dykyi, E.; Estoppey, N.; Fillmann, G.; Jantunen, L.; Kaserzon, S.; Maruya, K.A.; McHugh, B.; Newman, B.; Prats, R.M.; Tsapakis, M.; Tysklind, M.; van Drooge B.L.; Wong, C.S., 2024. AQUA-GAPS/MONET-Derived Concentrations and Trends of PAHs and Polycyclic Musks across Global Waters. Environmental Science & Technology, v. 58, 13456-13466. https://doi.org/10.1021/acs.est.4c03099.

Orellano, P.; Reynoso, J.; Quaranta, N.; Bardach, A.; Ciapponi, A., 2020. Short-term exposure to particulate matter (PM10 and PM2.5), nitrogen dioxide (NO2), and ozone (O3) and all-cause and cause-specific mortality: Systematic review and meta-analysis. Environmental International, v. 142. https://doi.org/10.1016/j.envint.2020.105876.

Ottaviano, G.; Pendolino, A.L.; Marioni, G.; Crivellaro, M.A.; Scarpa, B.; Nardello, E.; Pavone, C.; Trimarchi, M.V.; Alexandre, E.; Genovois, C.; Moretto, A.; Marani, M.; Andrews, P.J.; Marchese-Ragona, R., 2022. The impact of air pollution and aeroallergens levels on upper airways acute diseases at urban scale. International Journal of Environmental Research, v. 16, 4. https://doi.org/10.1007/s41742-022-00420-x.

Patel, P.N.; Jiang, J.H., 2021. Cloud condensation nuclei characteristics at the Southern Great Plains site: role of particle size distribution and aerosol hygroscopicity. Environmental Research Communications, v. 3. https://doi.org/10.1088/2515-7620/ac0e0b.

Pies, C.; Hoffmann, B.; Petrowsky, J.; Yang, Y.; Ternes, T.A.; Hofmann, T., 2008. Characterization and source identification of polycyclic aromatic hydrocarbons (PAHs) in river bank soils. Chemosphere, v. 72, 1594-1601. https://doi.org/10.1016/j.chemosphere.2008.04.021.

R Core Team, 2020. R: a language and environment for statistical computing. Versão 4.0.0. Vienna, Austria: R Foundation for Statistical Computing (Accessed September 20, 2024) at:. www.r-project.org.

Ravindra, K.; Sokhi, R.; Vangrieken, R., 2008. Atmospheric polycyclic aromatic hydrocarbons: Source attribution, emission factors and regulation. Atmospheric Environment, v. 42, 2895-2921. https://doi.org/10.1016/j.atmosenv.2007.12.010.

Requia, W.J.; Vicedo-Cabrera, A.M.; Amini, H.; Da Silva, G.L.; Schwartz, J.D.; Koutrakis, P., 2023. Short-term air pollution exposure and hospital

admissions for cardiorespiratory diseases in Brazil: A nationwide time-series study between 2008 and 2018. Environmental Research, v. 217. https://doi.org/10.1016/j.envres.2022.114794.

Rocha, L.D.S.; Correa, S.M., 2018. Determination of size-segregated elements in diesel-biodiesel blend exhaust emissions. Environmental Science and Pollution Research, v. 25, 18121-18129. https://doi.org/10.1007/s11356-018-1980-8.

Rodríguez-Cotto, R.I.; Ortiz-Martínez, M.G.; Rivera-Ramírez, E.; Mateus, V.L.; Amaral, B.S.; Jiménez-Vélez, B.D.; Gioda, A., 2014. Particle pollution in Rio de Janeiro, Brazil: Increase and decrease of pro-inflammatory cytokines IL-6 and IL-8 in human lung cells. Environmental Pollution, v. 194, 112-120. https://doi.org/10.1016/j.envpol.2014.07.010.

Rogula-Kozlowska, W.; Kozielska, B.; Klejnowski, K., 2013. Concentration, Origin and Health Hazard from Fine Particle-Bound PAH at Three Characteristic Sites in Southern Poland. Bulletin of Environmental Contamination and Toxicology, v. 91, 349-355. https://doi.org/10.1007/s00128-013-1060-1.

Sánchez-Ccoyllo, O.R.; Ynoue, R.Y.; Martins, L.D.; Astolfo, R.; Miranda, R.M.; Freitas, E.D.; Borges, A.S.; Fornaro, A.; Freitas, H.; Moreira, A.; Andrade, M.F., 2009. Vehicular particulate matter emissions in road tunnels in Sao Paulo, Brazil. Environmental Monitoring and Assessment, v. 149, 1-9. https://doi.org/10.1007/s10661-008-0198-5.

Silveira, R.S.; Correa, S.M.; Neto, N., 2022. Possible influence of shipping emissions on metals in size-segregated particulate matter in Guanabara Bay (Rio de Janeiro, Brazil). Environmental Monitoring and Assessment, v. 194, 828. https://doi.org/10.1007/s10661-022-10517-7.

Souza, C.V.; Corrêa, S.M., 2015. Polycyclic aromatic hydrocarbon emissions in diesel exhaust using gas chromatography-mass spectrometry with programmed temperature vaporization and large volume injection. Atmospheric Environment, v. 103, 222-230. https://doi.org/10.1016/j.atmosenv.2014.12.047.

Souza, C.V.; Corrêa, S.M., 2016. Polycyclic aromatic hydrocarbons in diesel emission, diesel fuel and lubricant oil. Fuel, v. 185, 925-931. https://doi.org/10.1016/j.fuel.2016.08.054.

Souza, S.L.Q.; Martins, E.M.; Correa, S.M.; Silva, J.L.; Castro, R.R.; Souza Assed, F., 2021. Determination of trace elements in the nanometer, ultrafine, fine, and coarse particulate matters in an area affected by light vehicular emissions in the city of Rio de Janeiro. Environmental Monitoring Assessment, v.193. https://doi.org/10.1007/s10661-021-08891-9.

Teixeira, J.; Delerue-Matos, C.; Morais, S.; Oliveira, M., 2024. Environmental contamination with polycyclic aromatic hydrocarbons and contribution from biomonitoring studies to the surveillance of global health. Environmental Science and Pollution Research, v. 31, 54339-54362. https://doi.org/10.1007/s11356-024-34727-3.

Verma, M.K.; Chauhan, L.K.S.; Sultana, S.; Kumar, S., 2014. The traffic linked urban ambient air superfine and ultrafine PM1 mass concentration, Contents of pro-oxidant chemicals, And their seasonal drifts in Lucknow, India. Atmospheric Pollution Research, v. 5 (4), 677-685. https://doi.org/10.5094/APR.2014.077.

Verma, P.; Stevanovic, S.; Zare, A.; Dwivedi, G.; Chu Vant, T.; Davidson, M.; Rainey, T.; Brown, R.J.; Ristovski, Z.D., 2019. An Overview of the Influence of Biodiesel, Alcohols, and Various Oxygenated Additives on the Particulate Matter Emissions from Diesel Engines. Energies (Basel), v. 12, 1987. https://doi.org/10.3390/en12101987.

Wang, P.; Zhu, S.Q.; Zhang, M.Y.; Shao, T.; Ying, Q.; Zhang, H.L., 2022. Atmospheric oxidation capacity and its contribution to secondary pollutants formation. Chinese Science Bulletin-Chinese, v. 67, 2069-2078. https://doi.org/10.1360/TB-2021-0761.

Wang, Q.; Liu, M.; Li, Y.; Liu, Y.; Li, S.; Ge, R., 2016a. Dry and wet deposition of polycyclic aromatic hydrocarbons and comparison with typical media in urban system of Shanghai, China. Atmospheric Environment, v. 144, 175-181. https://doi.org/10.1016/j.atmosenv.2016.08.079.

Wang, Q.; Liu, M.; Yu, Y.; Li, Y., 2016b. Characterization and source apportionment of PM2.5-bound polycyclic aromatic hydrocarbons from Shanghai city, China. Environmental Pollution, v. 218, 118-128. https://doi.org/10.1016/j.envpol.2016.08.037.

Wang, S.B.; Liu, G.J.; Yi, M.J.; Huang, X.M.; Zhang, H.; Hong, X.Y., 2022. The characteristics of particulate matter during an air pollution process revealed by joint observation of multiple equipments. Atmospheric Pollution Research, v.13, 8. https://doi.org/10.1016/j.apr.2022.101487.

Wang, Y.; Liu, H.; Lee, C.F.F., 2016c. Particulate matter emission characteristics of diesel engines with biodiesel or biodiesel blending: A review. Renewable and Sustainable Energy Reviews, v. 64, 569-581. https://doi.org/10.1016/j.rser.2016.06.062.

Zhang, J.; Cai, L.; Yuan, D.; Chen, M., 2004. Distribution and sources of polynuclear aromatic hydrocarbons in Mangrove surficial sediments of Deep Bay, China. Marine Pollution Bulletin, v. 49, 479-486. https://doi.org/10.1016/j.marpolbul.2004.02.030.

Zhang, J.; Lim, Y.H.; So, R.; Mortensen, L.H.; Napolitano, G.M.; Cole-Hunter, T.; Tuffier, S.; Bergmann, M.; Maric, M.; Shahri, S.M.T.; Brandt, J.; Ketzel, M.; Loft, S.; Andersen, Z.J., 2024. Long-Term Exposure to Air Pollution and Risk of Acute Lower Respiratory Infections in the Danish Nurse Cohort. Annals of the American Thoracic Society, v. 21, 1129-1138. https://doi.org/10.1513/AnnalsATS.202401-074OC.

Zhang, R.; Suh, I.; Zhao, J.; Zhang, D.; Fortner, E.C.; Tie, X.; Molina, L.T.; Molina, M.J., 2004. Atmospheric New Particle Formation Enhanced by Organic Acids. Science, v. 304, 1487-1490. https://doi.org/10.1126/science.1095139.